Development of a Mesoscale Ensemble Prediction System Using a Singular Vector Method

Kosuke Ono*, Yuki Honda*, Masaru Kunii**

**Numerical Prediction Division, Japan Meteorological Agency, Tokyo, Japan*

***Typhoon Research Department, Meteorological Research Institute, Tsukuba, Japan*

E-mail: kou.ono@met.kishou.go.jp

Since April 2007, we have been developing a mesoscale ensemble prediction system using a singular vector (SV) method to provide probabilistic information and multi-scenarios for operational mesoscale forecasting (MSM). To calculate perturbations, two singular vector methods are under trial. One is the mesoscale singular vector (MSV) method using the tangent linear model and its adjoint model based on the JMA nonhydrostatic model (JMA-NHM). The other is the global singular vector (GSV) method using the tangent linear model and its adjoint model based on the JMA global spectral model.

We are conducting four ensemble forecast experiments with different initial perturbations targeting the heavy rain associated with the Baiu front. First, we calculate the initial perturbations using the high-resolution MSV (with a horizontal grid spacing of 40 km and an optimization time of 15 hours: MSV40). The initial perturbations of MSV40 are more localized due to its higher resolution. These localized perturbations are effective in providing a suitable scale against the forecast of the mesoscale phenomenon, but are not effective for calculating scores estimated over a large verification area. For this reason, a combination of localized and non-localized perturbations is required. Accordingly, we calculate the low-resolution MSV (with a horizontal grid spacing of 80 km and an optimization time of 15 hours: MSV80). In order to combine the fine structure of MSV40 with the broad structure of MSV80, we blend MSV40 using a six-hour optimization time with MSV80 (BSV). Finally, for comparison, we use GSV with an optimization time of 24 hours. In all singular vector calculations, moist physics are used in the tangent linear and adjoint models, and the target area is the region around Japan (125 – 145°E, 25 – 45°N). Moist total energy is also used as the initial and final norm. Each ensemble forecast consists of 11 members (including a control forecast) using JMA-NHM with a horizontal resolution of 20 km.

Figure 1 shows the distribution of rainfall for observation and the six-hour forecast of the MSM along with the control forecast on 28 June 2008. The MSM and the control forecast, with horizontal resolutions of 5 km and 20 km, respectively, cannot predict the heavy rain around western Japan and the islands to the southwest. Figure 2 shows the ensemble spread of rainfall. A large spread for MSV40 and BSV is seen where light rainfall is predicted by the control forecast, while observed rainfall is heavy in other areas such as the islands to the southwest. It is suggested that the ensemble forecasts indicate the uncertainty of the control forecast and the potential area of observed heavy rain. Figure 3 shows the initial perturbations of each experiment. MSV40 has a fine structure, but is localized. MSV80 has a coarser and broader distribution than MSV40, and BSV has a fine and broad structure. GSV has the broadest structure. In this case, it seems that the size of the heavy-rain area is so small that only the experiments adopting initial perturbations with a fine structure can show heavy-rain potential.

Figure 4 shows the ROC area skill score for each experiment. The verification period is from 24 to 30 June 2008, and each initial is 18 UTC (a total of seven cases). In the first half of the forecast period, MSV80 is better than MSV40. MSV40 has a fine structure that is suitable for mesoscale phenomena, but as previously mentioned, in the case of a large verification area, it is inferior to MSV80. BSV can overcome this problem, and has the best score in the first half of the forecast period. In the latter half of the forecast, GSV is the best. This is because it has the broadest horizontal distribution and its perturbations are effective within the verification area in the latter half of the forecast period.

Next, to consider the uncertainty of the lateral boundary condition, we are developing lateral boundary perturbation using GSV as follows: Firstly, we calculate five GSVs, and then calculate a control run for the low-resolution JMA-NHM and five perturbed runs with a horizontal resolution of 40 km. Finally, we calculate the differences between the control run and the perturbed runs. Figure 5 shows an example of an ensemble forecast with lateral boundary perturbation. It can be seen that in the forecasted area of heavy rain near the boundary, the experiment with lateral boundary perturbation shows a large spread of three-hour accumulated precipitation (18 UTC July 2009, FT = 24). This is because lateral boundary perturbations affect the forecast

region through the lateral boundary. Combining the initial perturbations of MSV with the lateral boundary perturbations, we can expect an improvement of the score in the latter half of the forecast period.

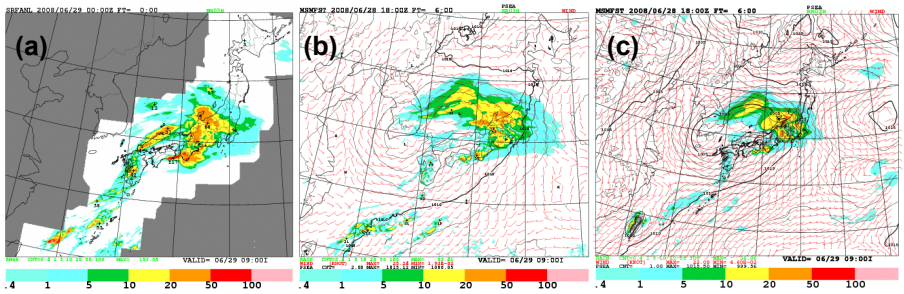

Fig 1. Distribution of three-hour accumulated precipitation [mm/3 h] at 00 UTC on 29 June 2009: (a) observation; (b) operational MSM (FT = 6); (c) control forecast (FT = 6)

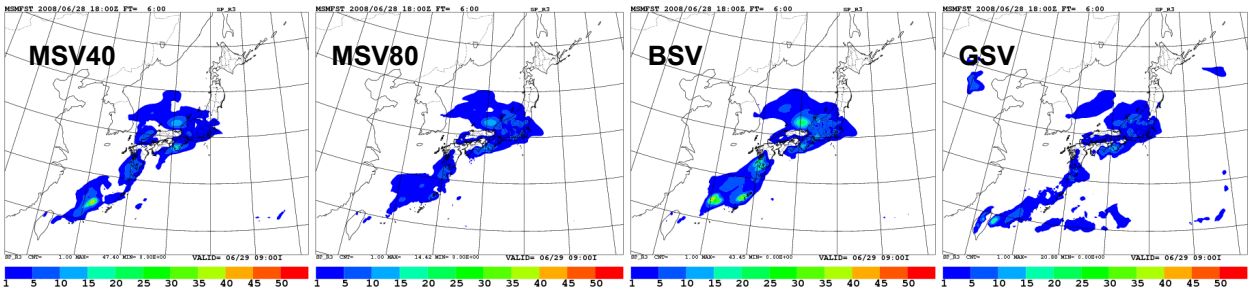

Fig 2. Ensemble spread of three-hour accumulated precipitation [mm/3 h]. FT = 6

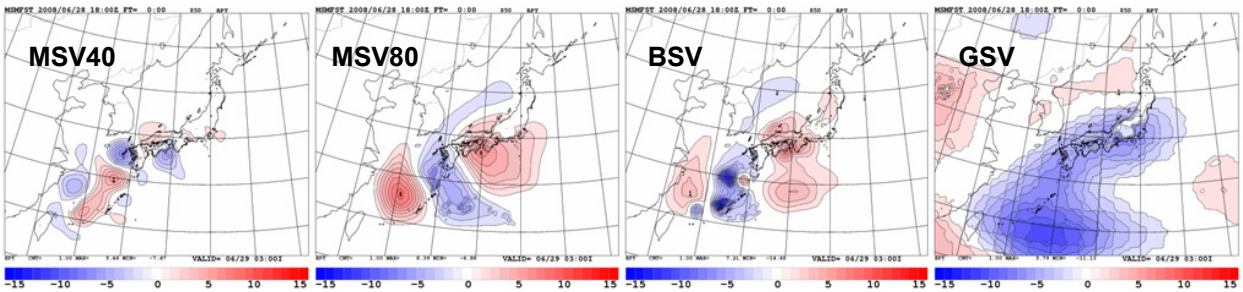

Fig 3. Initial perturbation of equivalent potential temperature at 850 hPa [K]

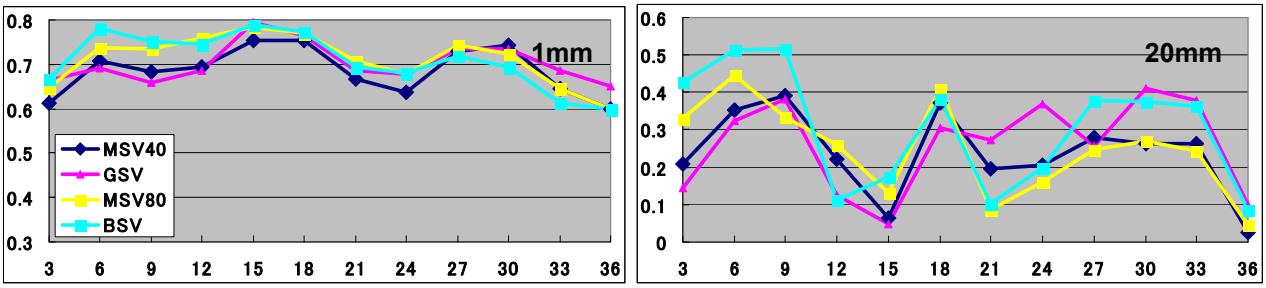

Fig 4. ROC area skill score for three-hour accumulated precipitation. The horizontal axis represents the forecast time.

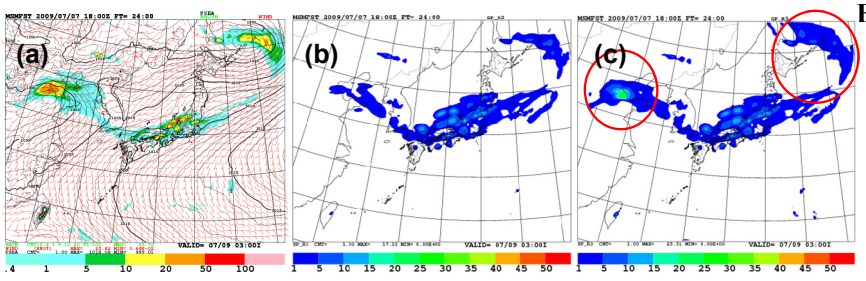

Fig 5. (a) Forecasted rainfall of the control run. (b) Ensemble spread of rainfall without lateral boundary perturbation [mm/3 h]. (c) As per (b), but with lateral boundary perturbation. The initial is 18 UTC on 7 July 2009. FT = 24.